LSST camera verification testing and characterization

Aaron Roodman, Andrew Rasmussen, Andrew Bradshaw, Eric Charles, Jim Chiang, Seth Digel, Richard Dubois, Tony Johnson, Steve Kahn, Shuang Liang, et al.

LSST Camera Testing and Characterization

A. Roodman[a,b], A. Rasmussen[a,b], A. Bradshaw[a,b], E. Charles[a,b], J. Chiang[a,b], S. W. Digel[a,b], R. Dubois[a,b], A. S. Johnson[a], S. Kahn[a,b], S. Liang[a,b], S. Marshall[a,b], H. Neal[a], K. Reil[a,b], K. Rykoff[a,b], R. Schindler[a,b], T. Schutt[a,b], Y. Utsumi[a,b], T. Bogart[a], T. Bond[a], B. Bowdish[a], S. Cisneros[a], A. Eisner[a], M. Freytag[a], D. Hascall[a], T. Lange[a], J. C. Lazarte[a], M. Lopez[a], C. Mendez[a], A. Plazas Malagon[a], S. Newbry[a], M. Nordby[a], D. Onoprienko[a], S. Osier[a], H. Pollek[a], B. Qiu[a], O. Saxton[a], S. Tether[a], G. Thayer[a], M. Turri[a], J. Banovetz[c], P. O'Connor[c], V. Riot[d], J. Wolfe[d], C. Lage[e], D. Polin[e], A. Snyder[e], A. Tyson[e], R. Nichols[f], S. Ritz[f], A. Shestakov[f], D. Wood[f], A. Broughton[g], H. Park[h], J. Esteves[i], A. Barrau[j], J. Bregeon[j], C. Combet[j], G. Dargaud[j], E. Lagorio[j], M. Migliore[j], F. Vezzu[j], P. Antilogus[k], P. Astier[k], G. Daubard[k], C. Juramy[k], D. Laporte[k], T. Guillemin[l], E. Aubourg[m], A. Boucaud[m], C. Parisel[m], F. Virieux[m], P. Breugnon[n], P. Karst[n], A. Marini[n], M. Fisher-Levine[o], and C. Waters[o]

[a]SLAC National Accelerator Laboratory, 2575 Sand Hill Road, Menlo Park, CA 94025, USA
[b]Kavli Institute for Particle Astrophysics and Cosmology, Stanford University, 452 Lomita Mall, Stanford, CA 94035, USA
[c]Brookhaven National Laboratory, 20 North Technology St, Upton, NY, 11973, USA
[d]Lawrence Livermore National Laboratory, 7000 East Avenue, Livermore, CA 94550, USA
[e]University of California, Davis, One Shields Avenue, Davis, CA 95616,USA
[f]University of California, Santa Cruz, 1156 High St., Santa Cruz, CA 95064, USA
[g]University of California, Irvine, Irvine, CA 92697, USA
[h]Duke University, Durham, NC 27708, USA
[i]University of Michigan, 500 S State St, Ann Arbor, MI 48109, USA
[j]Université Grenoble-Alpes, CNRS/IN2P3, Laboratoire de Physique Subatomique et de Cosmologie, 38026 Grenoble, France
[k]Sorbonne Université , Université Paris Cité, CNRS/IN2P3, Laboratoire de Physique Nucléaire et des Hautes Energies, 75005 Paris, France
[l]Laboratoire d¿'Annecy de Physique des Particules, Université Savoie Mont Blanc, CNRS/IN2P3, 74941 Annecy, France
[m]Université Paris Cité, CNRS, Astroparticule et Cosmologie, 75013 Paris, France
[n]Université Aix-Marseille, CNRS/IN2P3 , Centre de Physique des Particules de Marseille, 13288 Marseille, France
[o]Princeton University, Princeton, NJ, 08544, USA

ABSTRACT

The LSST Camera is the sole instrument for the Vera C. Rubin Observatory and consists of a 3.2 gigapixel focal plane mosaic with in-vacuum controllers, dedicated guider and wavefront CCDs, a three-element corrector whose largest lens is 1.55 m in diameter, six optical interference filters covering a 320–1050 nm bandpass with an out-of-plane filter exchange mechanism, and camera slow control and data acquisition systems capable of digitizing each image in 2 seconds. In this paper, we describe the verification testing program performed throughout the

Further author information: (Send correspondence to A.R.)
A.R.: E-mail: roodman@slac.stanford.edu, Telephone: 1 650 926 2705

Camera integration and results from characterization of the Camera's performance. These include an electro-optical testing program, measurement of the focal plane height and optical alignment, and integrated functional testing of the Camera's major mechanisms: shutter, filter exchange system and refrigeration systems. The Camera is due to be shipped to the Rubin Observatory in 2024, and plans for its commissioning on Cerro Pachon are briefly described.

Keywords: LSST Camera, Vera C. Rubin Observatory, CCD, Focal Plane

1. INTRODUCTION

The Vera C. Rubin Observatory is a new facility on Cerro Pachon in Chile designed to conduct the 10-year Legacy Survey of Space & Time (LSST), an all-sky optical/NIR survey of 18,000 deg^2 of the Southern Hemisphere in six optical bands.[1] The LSST will reach a 5σ limiting magnitude of roughly 27 (r-band) over 10-years and will observe each direction over 825 times. An estimated 20 billion galaxies, 17 billion stars and over 6 million solar system objects will be detected, enabling a wide range of scientific topics, from the precision study of Dark Energy and the accelerated expansion of the universe, the structure and formation of the Milky Way, to the history and development of the solar system. Images will be analyzed in real time to flag changes in flux or position of galaxies, stars or solar system objects, enabling extensive investigations in time-domain astronomy. We estimate that 10 million such alerts will be available to all Rubin community data-rights holders each night. All LSST data products will be available to data-rights holders as they are produced in annual data releases.

The Rubin Observatory's Simonyi Survey Telescope has a three-mirror modified Paul-Baker design, with an 8.4 meter combined primary-tertiary mirror and a 3.4 meter secondary. The optical system of telescope and Camera were designed in tandem, with astigmatism corrected by the three reflective elements, and the minimal power refractive elements primarily correcting chromatic aberrations. The resulting optical system delivers a fast $F/1.23$ beam with excellent optical performance across the entire 3.5° diameter field-of-view. The LSST Camera is the sole instrument for the Rubin Observatory, and it features a 3.2 gigapixel focal plane mosaic of CCDs with in-vacuum controllers, dedicated guider and wavefront CCDs, a three-element corrector whose largest lens is 1.55 m in diameter, six optical interference filters covering a 320–1050 nm bandpass with an out-of-plane filter exchange mechanism, and camera slow control and data acquisition systems capable of digitizing each image in approximately 2 seconds.

2. REQUIREMENTS & CAMERA DESIGN

The design of the LSST Camera is a product of the overall science goals of the LSST survey, as described in the Science Requirements Document.[2] From these, requirements were flowed down to all subsystems of the Rubin Observatory; a selection of the requirements for the Camera is presented in Table 1.

The LSST Camera requirements can be understood as flowing down from the need to survey rapidly, such that Rubin can observe every direction of the available night sky at the desired depth in just three or four nights. To achieve the needed etendue, Rubin features an 8.4 meter diameter primary mirror coupled with a 3.5° diameter field of view, and an extremely fast focal system with $F/1.23$. With this focal ratio a reasonable choice of 10 μm pixels yields a plate scale of $0.2''/pixel$ oversampling the typical PSF having FWHM of $0.7''$. These parameters lead to a focal plane with 201 CCDs and 3.2 Gigapixels and to achieve a high fill factor, 4kx4k CCDs with minimal uninstrumented area were developed. The very fast optical system necessitated a very flat focal plane to maintain good focus and image quality across the entire field of view. The needed survey speed also points to short exposures, with a nominal survey strategy of two 15 s exposures on a single field and a system capable of rapid slewing. To minimize dead-time, a goal of a two second read-out was specified, which led to the development of custom 16-channel CCDs operating at 0.5 MHz. In turn the large number of video channels ($201 \times 16 = 3216$) led to the placement of custom high-density CCD controllers immediately behind the focal plane and in the same vacuum vessel, so that only power and digital data connections are needed through the cryostat vacuum. The imaging region is comprised of 21 Science Rafts each with 9 Science CCDs, and 4 Corner Rafts each with 2 Guider CCDs and one split Wavefront CCD. The large focal plane (64cm by 64cm) required a refrigeration system with 500 Watts of lift at −130 deg C to cool the CCDs (Cryo Refrigeration), and an additional refrigeration system to cool the in-vacuum controller electronics with 1000 Watts of lift at −40 deg C

Table 1. A selection of LSST Camera requirements. The top set are Camera level requirements, and bottom pertain to the Focal Plane and Cryostat.

Requirement	Criteria
Optical Throughput	$> 22.5\%, 45.4\%, 49.1\%, 46.3\%, 12.6\%$ in (u,g,r,i,z,y) bands
Camera contribution to Image Quality	< 0.3 arcsec FWHM
Readout Time	2 (3) seconds
Shutter Light Tightness	$< 0.1\, e^-$/pixel per 15 sec in dark dome
Shutter Timing Repeatability	< 50 msec
Guider Readout Rate	> 9 Hz with 50×50 pixel ROI
Filter Exchange Time	< 90 sec
Mass	< 3060 kg
Quantum Efficiency	$> 41\%, 78\%, 83\%, 82\%, 75\%, 21\%$ in (u,g,r,i,z,y) bands
Focal Plane Flatness	$\pm 11\, \mu$m
CCD Diffusion	$\sigma < 5\, \mu$m
Read Noise	$< 9(13)\, e^-$ RMS
Crosstalk	$< 2 \times 10^{-3}$ ($< 1 \times 10^{-4}$) intra- (inter-) Raft
Gain Stability	$< 1\%$ RMS over 12 hours, $< 0.1\%$ RMS over 1 hour
Linearity	$< 3\%$ up to Full Well
CCD Temperature Stability	± 0.25°C variation over 12 hours

(Cold Refrigeration). Finally, the placement of the Camera inside the annulus of the secondary mirror (M2) required an extremely compact and light weight design, with no components outside the edge of the Camera's large L1 lens (1.55 m diameter) and all support equipment in a narrower Utility Trunk fitted inside the M2 support structure. With these space constraints, the only place to store the large (80 cm diameter) filters is around the perimeter of the Camera body and outside the cryostat and the Filter Exchange system must move the filters in three dimensions. Likewise, the Shutter features two overlapping panels on each side of the aperture, to fit in the Camera envelope.

3. VERIFICATION TESTING PROGRAM

The goals of our Camera testing program have been multi-fold: to verify Camera requirements and also to gain ample experience in operating the Camera prior to its installation in the Rubin Observatory, to optimize its performance and especially to uncover problems as early as possible. Therefore we adopted an approach to conduct testing of each subsystem and at each stage of the Camera integration (*test-as-you-go*) and to perform the testing in as realistic a manner as possible (*test-as-you-use*). In addition, we took advantage of the Rubin Observatory's systems engineering and requirements flow-down to trade off performance parameters where necessary. A previous proceeding described the verification testing program in the planning stages[3,4] The final Camera mechanical integration will be described in a companion proceeding at this conference.[5]

As an example, we point to the range of CCD and Focal Plane testing conducted. Our custom CCDs were all tested at the vendor, and a subset were individually tested with commercial controllers to ensure consistency with the vendor measurements[6,7] The CCDs were assembled into 21 9-CCD sub-assemblies (Science Rafts) and 4 3-CCD units with wavefront and guider sensors (Corner Rafts). Each Raft, with accompanying controllers on custom Readout Electronics Boards (REBs) was tested at BNL[8] and again after shipment to SLAC. Testing at both sites enabled more rigorous testing and higher throughput, and allowed us to incorporate improvements in CCD bias and clock voltages, sequencer micro-code, and image collection and analysis during the Raft production

period. Next, we installed rafts into the cryostat focal plane in three stages, first with two engineering grade rafts, second with the focal plane partially filled with 9 Science Rafts and all 4 Corner Rafts and finally with the completed Focal Plane. Electro-optical testing and focal plane height measurements were performed as part of each of these three phases, again to ensure that the installation was proceeding as desired and to identify problems as soon in the construction cycle as possible. Due to problems with the original design of the Cold refrigeration system, responsible for cooling the in-vacuum REBs, we added an additional phase of testing with the completed Cryostat attached to the Utility Trunk and its support equipment. Lastly we conducted a round of testing with the completed Camera.

Electro-optical Focal Plane verification testing was conducted with a number of light projectors, both to cover all pixels with roughly uniform illumination and also with structured light sources on individual CCDs for more detailed studies of CCD performance. Two different uniform illuminators were used, each with an integrating sphere and projector lens placed in front of the Cryostat or Camera. The initial projector used a commercial Xe lamp with either broad-band or narrrow-band filters, while a second device used a set of six LEDs with wavelengths centered on the Camera's filter bandpasses. A photodiode with picoammeter readout monitored the flux level for each exposure. Additional structured light projectors were capable of producing a grid of artificial stars, four large spots or a single streak to study cross-talk, and a wavelength selectable pencil beam. These projectors were mounted on moveable stages to place light as desired on the Focal Plane. The pencil beam had a photodiode that could be inserted into the beam to enable calibrated flux throughput measurements and was mounted an a 4-axis stage to produce any ray hitting the focal plane from any portion of the pupil.

Custom scripts were developed to collect bias, dark and flat-field image sequences with flexible specification of the number, exposure time, flux level and wavelength. Images were transferred into the Rubin U.S. Data Facility at SLAC and an appropriate subset of the Rubin Data Management instrument signature removal algorithms was applied. Additional analysis code was developed to assess a selection of key performance parameters for each of the 16 amplifier sections of the CCDs, these included read noise, gain, full-well, charge transfer inefficiency, dark current as well as summary statistics such as temporal bias variation, gain variation and brighter-fatter correlations. Mosaics of these quantities across the Focal Plane and summary histograms were produced, accessible from a static web interface for rapid perusal of all 201 CCDs. Image mosaics from bias, dark and flat fields were also produced.

Additional verification testing was performed to measure the height of the focal plane and the optical alignment of the L1-L2 lens pair with respect to the vacuum window L3 and the Focal Plane, as contributions to image quality requirements. A custom metrology device was developed using non-contact height sensors, a moveable stage and a reference optical flat to measure the relative heights of the CCD surfaces. Optical alignment was performed with standard laser tracking using spherically mounted retro-reflectors on the lens cells and cryostat, making use of vendor-provided fiducialization. Timing requirements for the shutter, filter exchange system and guiders were verified with functional testing. The Camera's control system records very extensive telemetry, including CCD and REB temperatures, to enable verification of thermal requirements.

3.1 PROBLEMS DISCOVERED DURING TESTING PROGRAM

During the course of Camera integration and testing, four major problems were uncovered and remedied. Each of these was found during the verification testing program, and they were discovered at an early time in the integration, which of course gave us more time in our schedule to mitigate these problems. These issues were: particulate contamination produced in Raft assembly that shorted out CCD wire-bond or connector pins, failure of the vapor-compression Cold Refrigeration system responsible for cooling the REBs to $-40°C$, a vacuum leak in a REB power-supply vacuum feed-through and failure of the turbo-molecular pump on the main Cryostat.

4. VERIFICATION TESTING RESULTS

In this section we present a selection of testing results, both for requirement verification and also Camera characterization. First light for the completed Focal Plane was achieved in the fall of 2020, and publicity images were produced with a *pin-hole projector* consisting of a small light-tight box with a 150 μm pinhole internally lit with battery-powered LED lights, placed roughly 1 meter below the Focal Plane. An image of anything in the

box is projected onto the CCDs; our first light images were of a well-known photograph of Vera Rubin and of a piece of Romanesco broccoli, as shown in Figure 1.

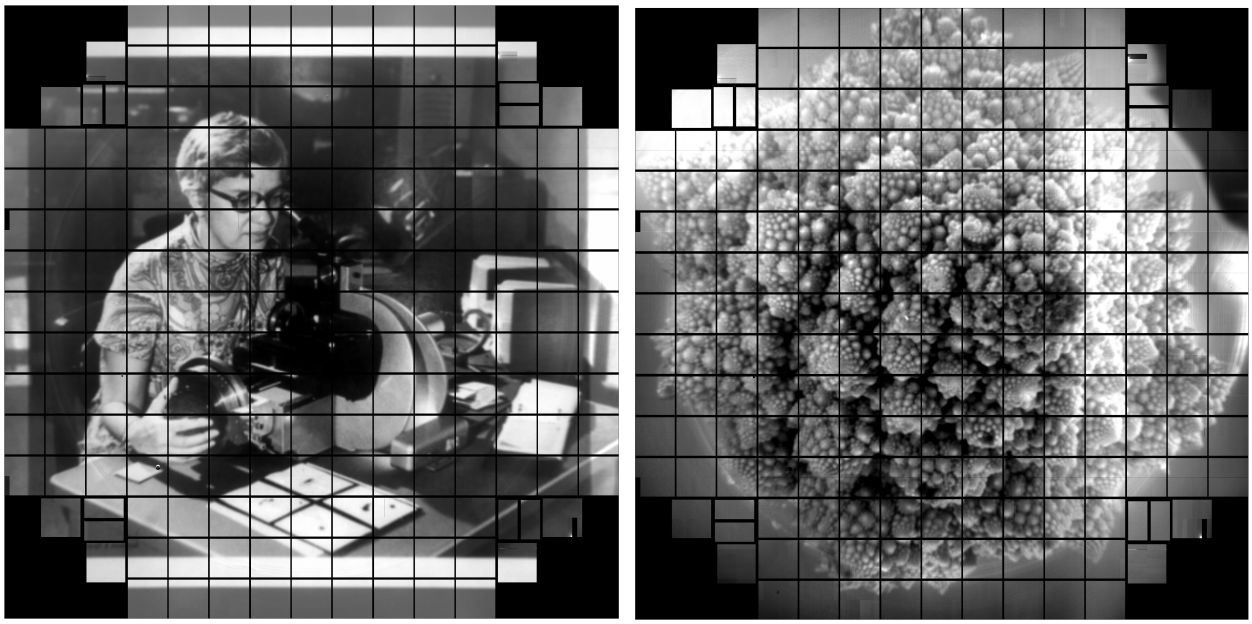

Figure 1. First light Focal Plane pin-hole projector images of Vera Rubin (left) and Romanesco broccoli (right).

4.1 Quantum Efficiency & Throughput

The quantum efficiency of the CCDs was measured for each Science Raft in a dedicated test stand.[8] QE results are shown for all 189 CCDs as a function of wavelength in Figure 2. The sensors were produced by two vendors and their different anti-reflective coatings produced slightly different results; these differences will be corrected via in-dome calibration measurements. Integrated throughput requirements were verified by combining the CCD QE results with vendor provided throughput in both the optical filters and the three lenses. This combination in shown in Figure 2. The Integrated throughput exceeds the required level with more than 30% margin in each filter band. We explicitly measured the integrated throughput for the Camera system in the r filter, using the wavelength-selectable pencil beam. Those measurements compare well with the combined values, as shown in Figure 2.

4.2 Image Quality

Three components contributing to image quality are the subject of verification testing: CCD diffusion, focal plane height variations, and optical alignment. Additional contributions from the as-built lens figure and wavefront are also assessed from vendor measurements and optical modeling.

The typical level of CCD diffusion is $\sigma \sim 4.3\,\mu$m as measured with Fe^{55} x-rays, corresponding to a FWHM contribution of $0.20''$, which is the dominant contribution from the Camera to image quality. Verification testing at the cryostat stage used a flat window instead of the L3 lens mounted to a ring with Fe^{55} sources and shutters placed around the ring perimeter. A mosaic of the CCD diffusion is shown in Figure 3 measured with the completed focal plane.

Due to the Rubin Observatory's fast $F/1.23$ optical system, deviations from a flat Focal Plane will quickly impact image quality. Each component of the Focal Plane had tight height specifications, including the CCDs, Raft baseplates and Raft mounting structure (Grid). The Grid was attached to the Cryostat via a kinematic mount with flexures, which were adjusted to place the CCD surface at the desired location relative to the Cryostat front face where the L3 lens was mounted. Each Raft was constructed to provide a flat CCD surface at

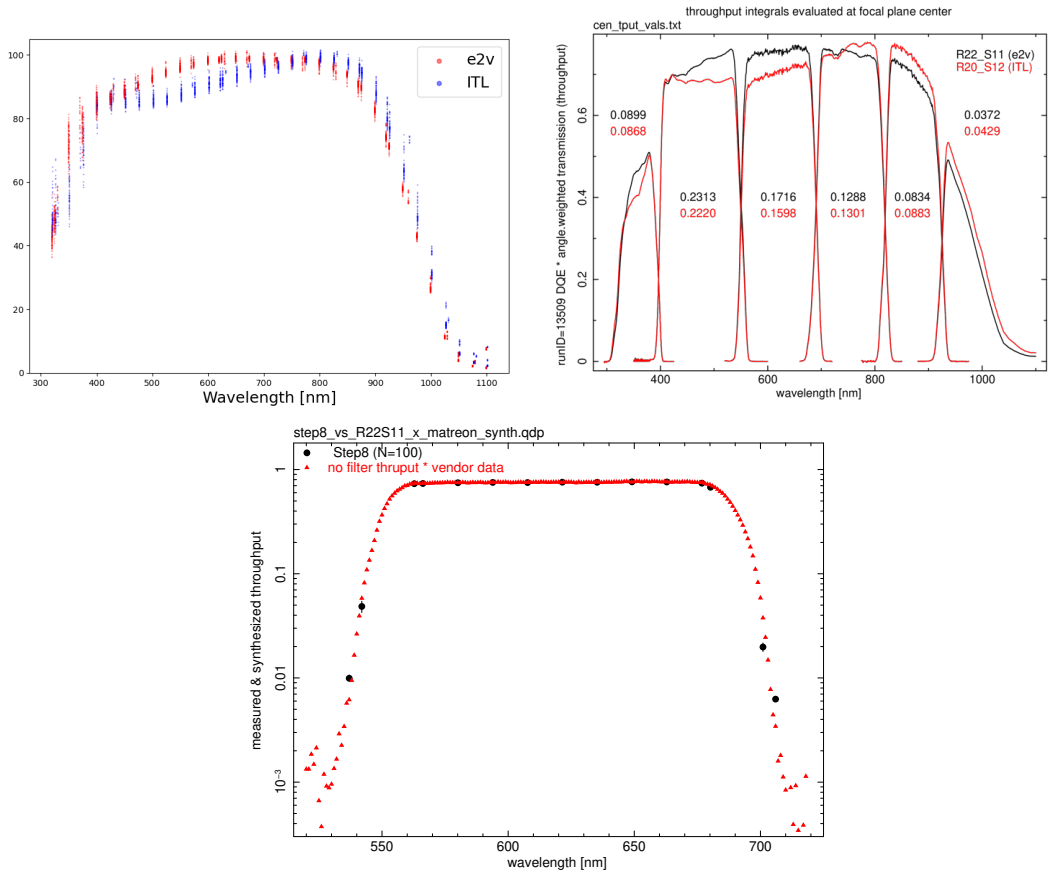

Figure 2. Quantum efficiency as a function of wavelength for each of the 189 Science CCDs (upper left). CCD-250 sensors from e2v are shown in red, STA-3800 sensors from ITL are shown in blue. Integrated throughput, combining our CCD measurements with vendor filter and lens throughput data, as a function of wavelength (upper right). Integrated throughput measurements in the r-band as a function of wavelength, compared against the combined values (bottom).

the desired height above the kinematic mounting points between the back of the Raft baseplate and the Grid, and each Raft's height was individually measured with a custom metrology instrument. Precision tooling balls were used between Grid cones and Raft v-blocks; different size balls were available for individual height adjustment but ultimately only tooling balls of the nominal size were used. The focal plane surface was measured with a custom metrology instrument, with precision non-contact height measurement devices placed on an XY stage and referenced to a moveable optical flat.[9] The focal plane surface was measured at room temperature without the flat window installed, at room temperature with the flat window and finally with the CCDs cooled to their nominal -100° C temperature. A map of the relative height at operating temperature is shown in Figure 4, along with histograms of the relative height distribution for Science CCDs, Wavefront CCDs and Guider CCDs. Notably the RMS height variation in the Science CCDs is 4.0 μm with a roughly Gaussian distribution, consistent with the image quality allocation for this contribution. The Wavefront sensors in the Corner Rafts have two CCDs split so that one half is above or below the Focal Plane by 1.5 mm. This offset is removed for the Focal Plane height map and histogram, with only relative deviations shown.

The delivered image quality of the Rubin optical system was evaluated using the as-built wavefront and positions of the three mirror system as well as the measured locations of the L1-L2 lenses, L3 and the focal plane following optical alignment of the L1-L2 lens pair. The L1-L2 pair is mounted to the Camera body *front flange* via six adjustable legs, whose lengths were set during the laser tracking based alignment of L1-L2 to optimize the delivered image quality of the entire Rubin optical system. Spot diagrams, in the r-band, for twelve

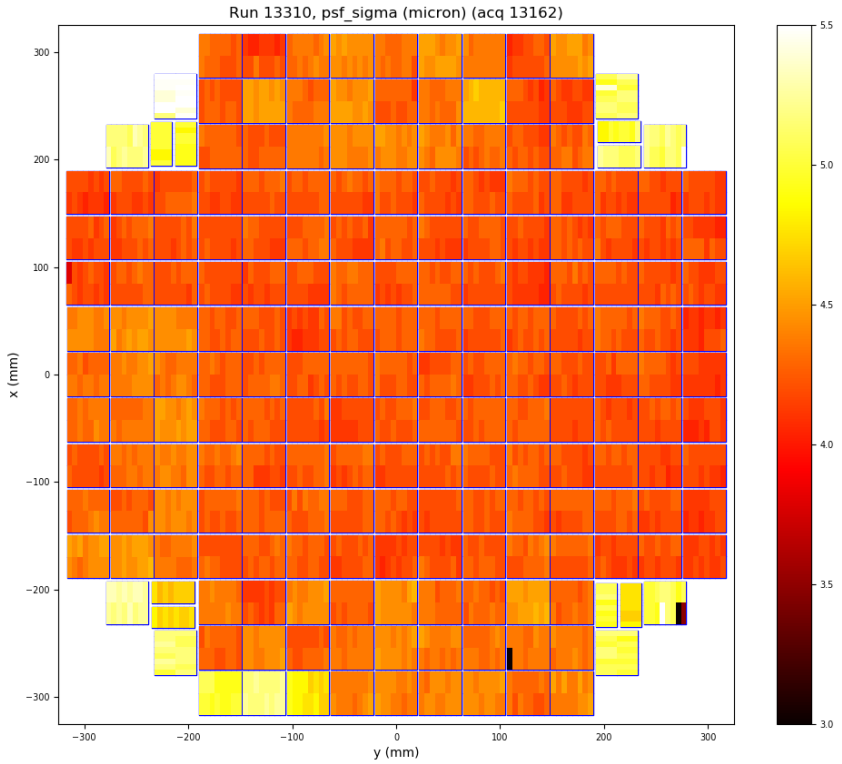

Figure 3. Diffusion σ in each CCD, as measured via Fe^{55} x-rays. All science CCDs are operated with a back bias of 50 V, except for three CCDs in the lower left of the focal plane which are set at 30 V to minimize the flux from a hot defect. The wavefront and guider CCDs are set to 30 V back bias. The observed diffusion is consistent with expectations given the back bias and the 100 μm thick Si.

fields and five wavelengths are shown in Figure 5 for both the Rubin design parameters and the as-built system. Note that the as-built image quality is optimized using the 10 degrees of freedom available in the Camera and M2 hexapods. The Rubin active optics system will adjust these degrees of freedom and 38 additional ones for the M1-M3 and M2 mirror figures with both static look-up tables and an active control loop, so assessing the image quality after just a partial optimization is a conservative choice. The contribution in quadrature of the as-built Camera optics to image quality, including measured lens wavefronts and misalignments, was just 0.079″, consistent with the allocation.

4.3 Timing Requirements

The nominal cadence of image taking in LSST consists of two exposures (snaps) taken on the same field (visit). Individual steps for each visit are listed in Table 2, which compares the design values with the as-built timing. The shutter is opened moving in one direction across the aperture and closed moving in the opposite direction, such that each part of the field of view is exposed for an identical duration; as such only one shutter movement needs to be included for each snap. In addition, only one CCD readout is included since the readout of the second snap occurs while the telescope is slewing to the next field. The excess time relative to nominal of 0.4 seconds is mostly due to the choice of a 2.407 second readout. A nominal 2.0 second readout was demonstrated, but better noise and full well performance was achieved with a slightly longer readout time. The estimated depth for the full 10-year LSST survey was evaluated to compare better performance but with slightly longer time for each

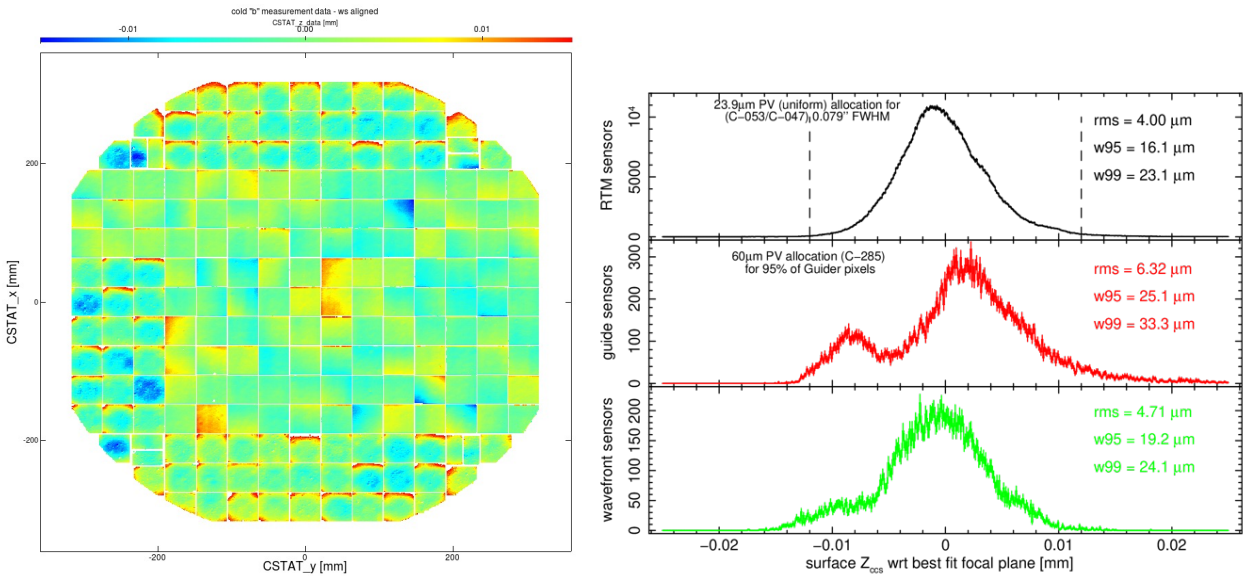

Figure 4. Measured relative height map of the Focal Plane (left). Relative height distributions for Science, Guider and Wavefront CCDs (right).

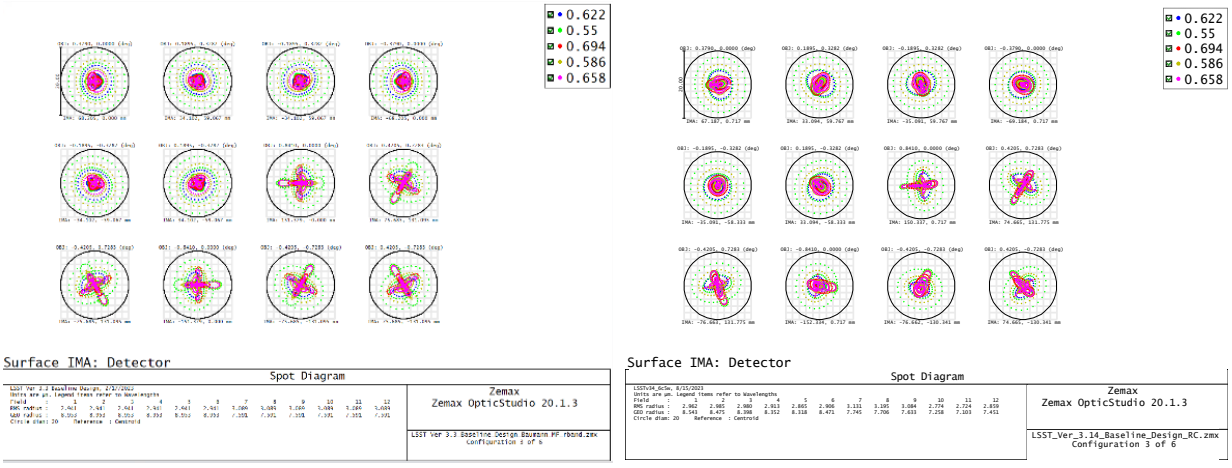

Figure 5. Optical ray tracing spot diagrams for the Rubin optical design (left) and the as-built system (right), for twelve fields and five wavelengths in r-band. The as-built results are following an optimization of the image quality with the Camera and M2 hexapod degrees-of-freedom.

visit and the change was shown to lead to a modest net gain. In principle, further optimization is possible, in particular to perform the CCD clear for the first snap at the end of the slew, but this awaits commissioning of the Rubin Observatory.

In addition to the overall visit timing, we verified the requirement on the variation of exposure time across the field of view caused by differences in the shutter trajectories for the opening and closing motions. The shutter blade trajectories are measured by both motor encoders and Hall probe sensors placed at intervals along the shutter rail. Both telemetry streams are recorded for each shutter motion by the Camera control system, and are fit to a simple physical model to aid in monitoring. The difference in time of the open and close trajectories versus position is shown in Figure 6(top) for both starting shutter blade positions. The spikes at the edges are outside the aperture of the LSST beam, and the region inside the beam shows extremely uniform exposure times across the field of view, at the 1 msec level, almost a factor of 50 better than required. We also show 50 shutter

Table 2. Timing of steps in a nominal LSST set of two exposures (visit) on a single field.

Step	Design Values [sec]	As-Built Values [sec]
Shutter Movement	2×0.980	2×0.9
Shutter Open	2×15.0	2×15.0
CCD Clear	–	2×0.065
Readout	2.0	2.407
Camera control & DAQ overhead	0.040	0.072
Total	34.0	34.411

trajectories in Figure 6, demonstrating good repeatability.

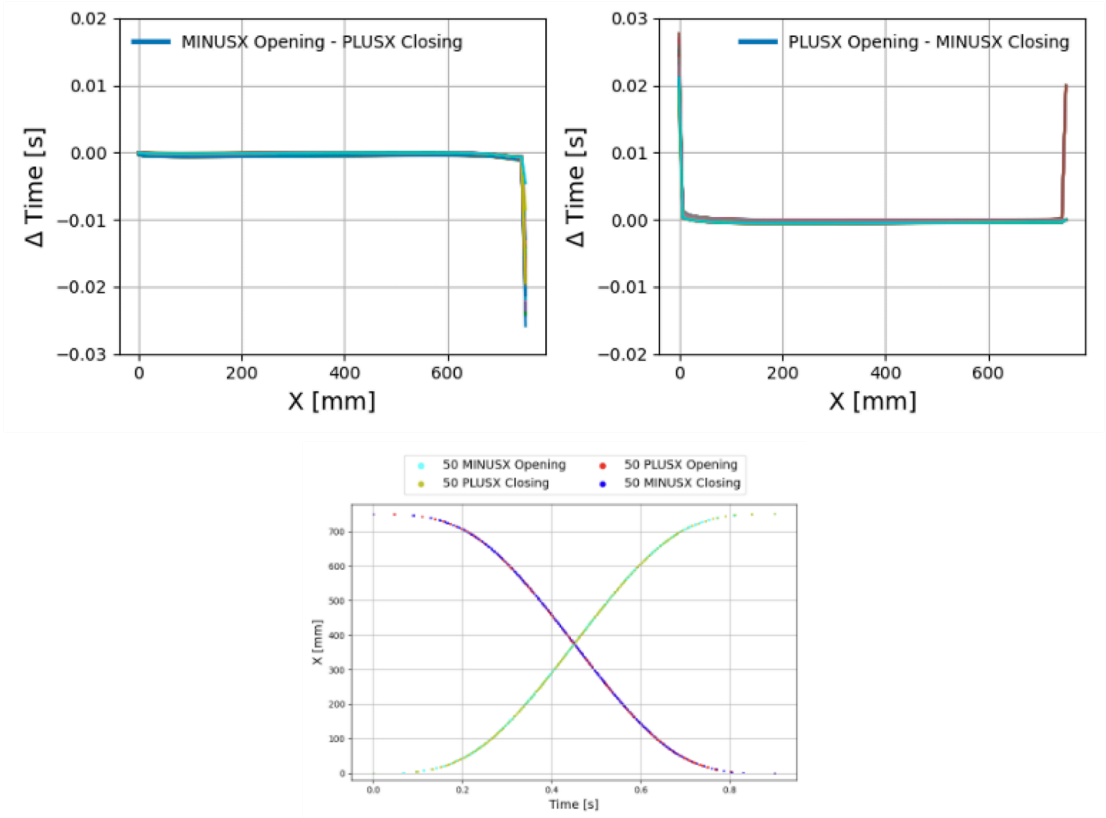

Figure 6. Difference in exposure time vs. position for shutter open/close trajectories, for both shutter starting positions (top). Shutter trajectories from 50 open/close cycles in both starting positions (bottom).

Two minutes are allotted for filter exchanges, with up to 30 seconds to rotate the Camera to its nominal orientation where the Filter Exchange mechanism is upright, and another 90 seconds for the filter exchange itself. The Filter Exchange system.[10] first moves the filter from its online position to the carousel located around the Cryostat, next the carousel is rotated either one or two slots in either direction to bring the desired filter into position, and finally the filter is brought down to the online position. A histogram of the filter exchange timing is shown in Figure 7, demonstrating motion within the allocated time. The two peaks are for cases where the carousel rotates either one or two slots to bring the desired filter online.

The final timing specification is for the Guider CCDs readout. There are two Guider CCDs in each of the

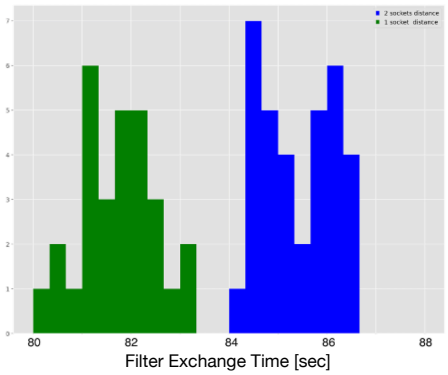

Figure 7. Filter exchange timing for 100 exchanges.

four Corner Rafts; these are STA-3800 devices identical to those used as Science CCDs. The Guider CCDs can be readout in full frame mode along with the rest of the Focal Plane for calibrations, but in nominal use have a 50×50 pixel region-of-interest (ROI) readout at 9 Hz. Each Guider CCD may have a different ROI as specified by the Observatory Control System, and the ROI may cross amplifier boundaries in the top or bottom half, but not the mid-line break of the CCDs. A single ROI from laboratory testing with an artificial star and from the Rubin Auxiliary Telescope (AuxTel) is shown in Figure 8. The Guider has achieved 8.8 Hz ROI operation in this testing, and a final suite of requirements for read noise and ROI placement and size will be verified when the Camera is operated in the summit facility in the third quarter of 2024.

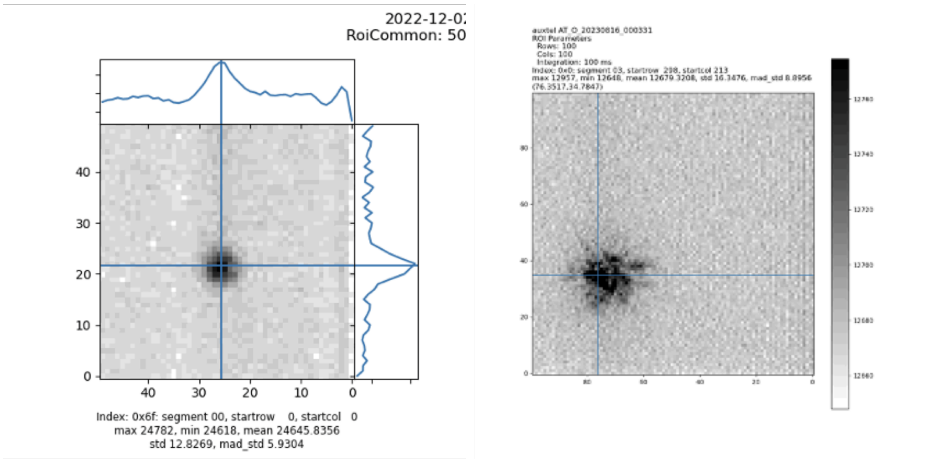

Figure 8. Guider CCD region of interest for an artificial star (left) and a star observed with the Rubin Auxiliary Telescope (right). The axes are labeled in pixels.

4.4 Electro-Optical Testing & Results

Many of the Camera requirements depend on the Focal Plane performance in electro-optical testing. Measurements of quantities such as read noise, linearity, full-well, gain and gain stability and charge transfer inefficiency were made at each step of the Camera construction. Here we show results from the electro-optical testing periods from October to December of 2022 with the Cryostat only and from June and November of 2023 with the fully assembled Camera. A mosaic of the read noise and cumulative histogram of the noise is shown in Figure 9(left). A subset of CCD amplifier channels exceeded the requirement of $9e^-$ RMS, and again the impact of this was evaluated against the LSST Science requirements, with the conclusion that the higher noise on a small number of channels would have little impact except for a small reduction in depth for u-band images, especially on

consideration that most of the CCDs achieved less than $6e^-$ RMS noise. The read noise requirement was recast with allotments at 7, 9, 13 and 18 e^- RMS noise levels and the measured cumulative read noise levels are shown in Figure 9(right). The read noise levels were highly consistent across electro-optical testing from single Raft through to full Camera operation.

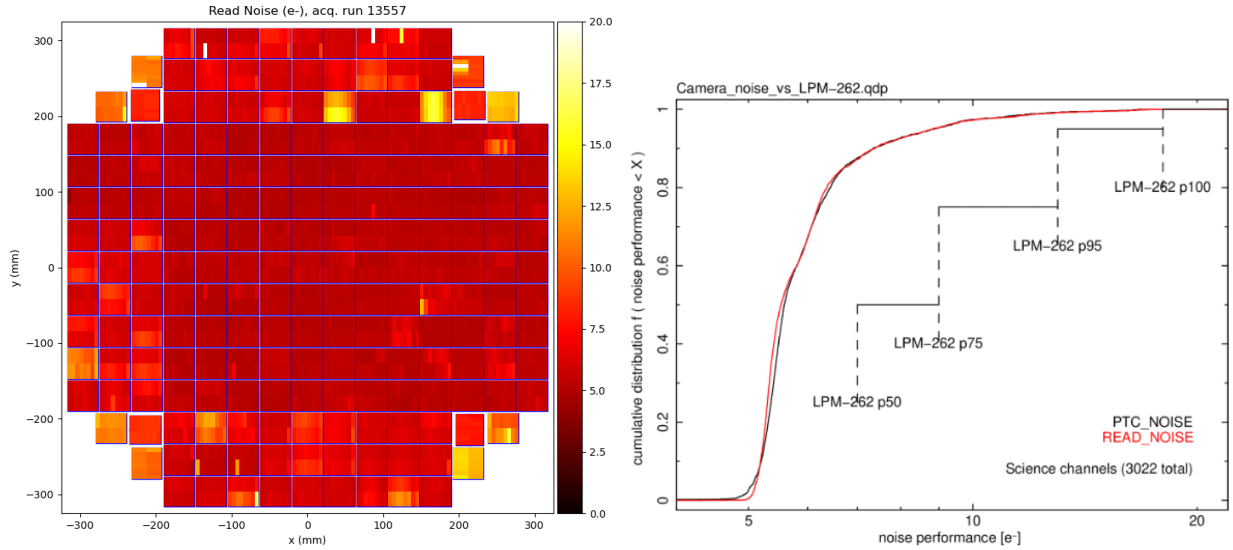

Figure 9. Read noise mosaic (left) and cumulative distribution of read noise levels (right) in units of RMS electrons.

The level of cross talk between readout channels was measured with structured light sources during electro-optical testing at the Cryostat level. Cross talk results shown here come from images with four large light spots projected onto different parts of four amplifiers (individual ∼1M pixel readout segments of one sensor), such that the spots occupy different pixels on each amplifier.[11] This 4-spot pattern was imaged four times per CCD (to cover all 16 readout segments) and on all CCDs in the Focal Plane. Care was taken to model stray light and diffraction tails overlapping the pixels where cross-talk is observed. No cross-talk was observed between CCDs, only internally in each CCD. The matrix from source amplifier to target amplifier is shown in Figure 10 (left) for a representative CCD from each vendor, and histograms of all cross-talk coefficients are shown in Figure 10 (right) for different groupings of amplifiers. In each case the cross talk level is shown for a flux level of roughly $50ke^-$. The level of cross talk is roughly 2×10^{-4} for nearest-neighbor amplifiers and drops off with distance. In this analysis the cross talk is analyzed in terms of a single coefficient, but as mentioned below further studies show a nonlinear cross talk component as well as small time-dependent effects. The cross talk level is substantially lower than the required level and the lack of any inter-CCD cross talk reduced the complexity of the needed corrections.

The gain of the video chain is measured via the photon transfer (PTC) method, using over 800 images with a logarithmic distribution of flux at lower values and evenly spaced fluxes at higher values. The flat fields are analyzed taking into account the impact of the brighter-fatter effect on PTC.[12] A mosaic of the measured gain is shown in Figure 11(left). Gain values differ between the two CCD types, but are quite consistent for each. A single group of three CCDs in the lower left is out of family due to differences on the REB board that controls them. The PTC gains are highly consistent between different operating periods. We monitor the gain stability over time with sequences of flat field images at a constant flux, with corrections from the photodiode monitoring the light source. Relative response from a sequence of flat fields taken over 24 hours is shown in Figure 11(right) with one panel per Raft and results from different CCDs shown in different color points. The normalized response is stable at a level better than 0.05%, much better than the Camera requirements. A few out-of-family points appear in all CCDs presumably due to common-mode photodiode deviations. Two CCDs have single amplifiers with very low response, the plots include this data with its higher level of variation. There is a very small gain response variation present, due to a small changes in temperature at the REBs. The REBs are measured to

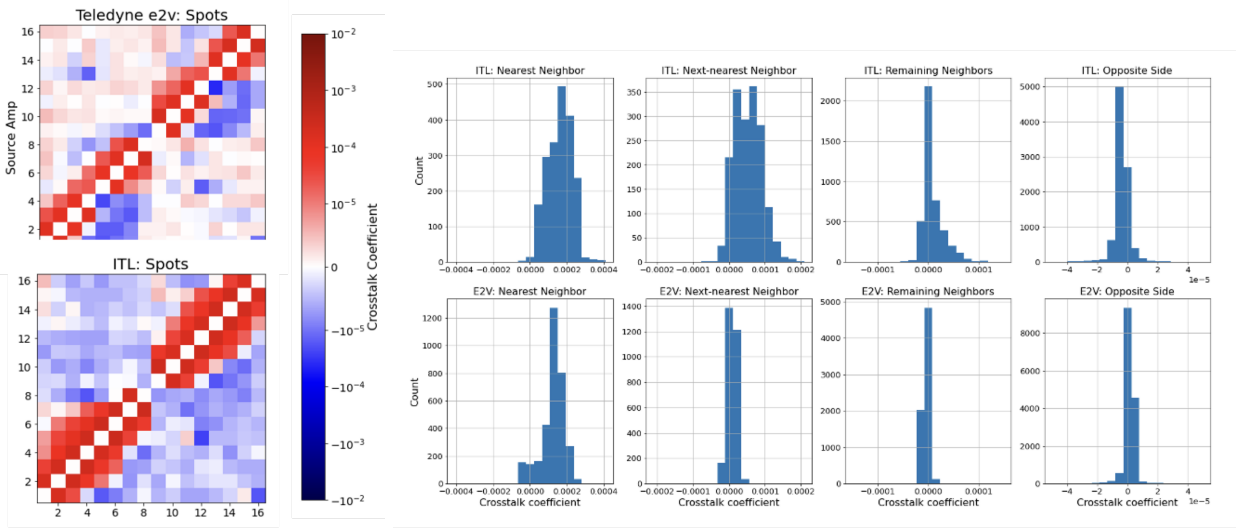

Figure 10. Cross talk coefficient matrix between source and target amplifiers on a single CCD for each CCD type (left) and distribution of the cross talk coefficients for nearest neighbors, next-nearest, other amplifiers on the same CCD half and amplifiers on the opposite CCD half (right).

have a temperature coefficient of roughly 0.06% per degree °C which will be applied as an Instrument Signature Removal (ISR) correction using REB temperatures from telemetry if necessary.

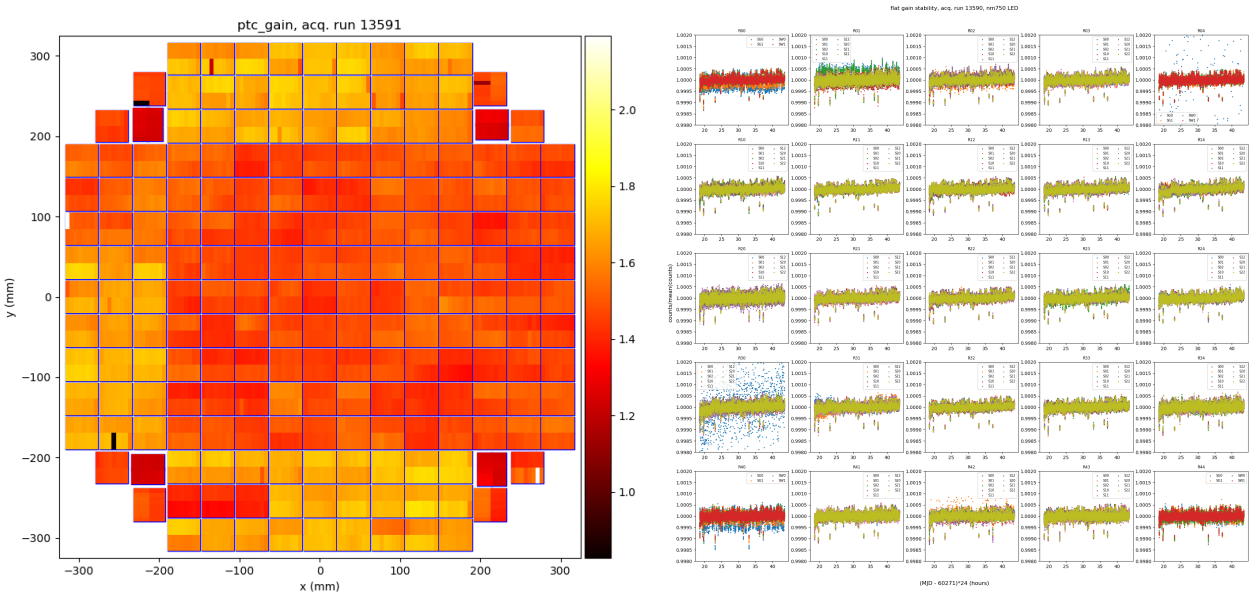

Figure 11. Gain mosaic in units of $[e^-/\mathrm{ADU}]$ measured with the photon transfer method (left) and relative Gain stability from flat field images taken over a 24 hour period (right).

We also evaluate the CCD full-well with the same set of PTC flat-fields. We evaluate several full-well measures, but cite the maximum observed signal, as shown in the mosaic in Figure 12(left). We also record a measure of the deviation from the PTC curve and the linearity of response; each of these are different and may be used in image analysis as needed by the ISR algorithms. We produce individual PTC and linearity plots for each CCD amplifier; examples of the linearity and linearity residuals for a sample CCD are shown in Figure 12(middle) and

(right). The linearity results in this case are affected by low signal-to-noise photodiode monitoring signals at low flux, an issue we plan to remedy during Camera reverification on Cerro Pachon as described in the conclusion. Here we collect images at three different LED current levels, and find that the ratio of CCD/Photodiode flux is slightly different for each. We collect images that overlap in flux at each LED current, and apply a normalizing correction between the levels.

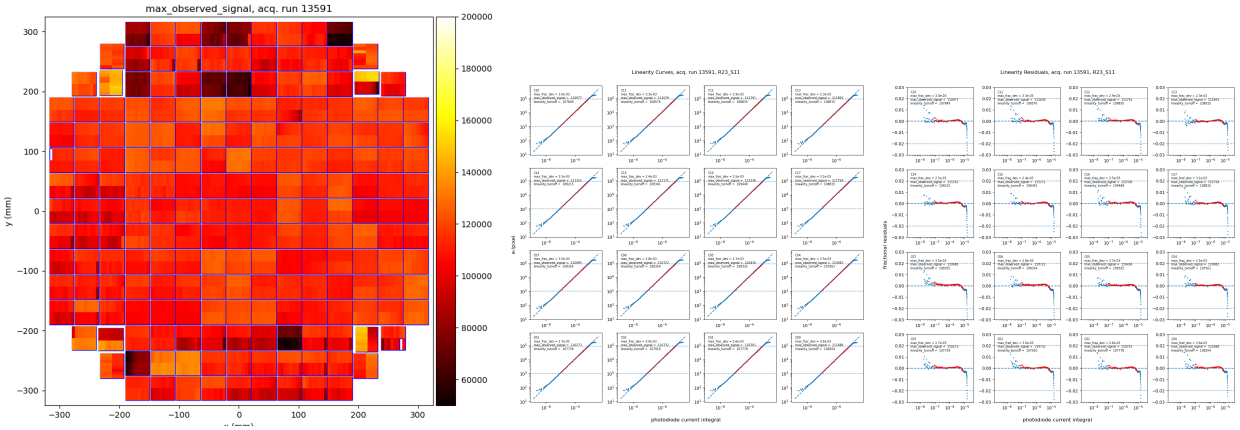

Figure 12. Full Well mosaic $[e^-/ADU]$ from flat fields (left), Linearity of measured signal in ADU versus monitoring photodiode flux (middle) and Linearity residual after a linear fit (right).

We demonstrate the required temperature stability using Camera telemetry, measuring CCD and REB temperatures as a function of time, as shown in Figure 13. The CCD temperature is stable to better than the required level of 0.25° C over this entire period, although we note that individual readings are noisier than this level of precision so averaging over periods of several minutes is needed. The REB temperature is stable to better than 1.0° C during periods when either images are being taken or when the Camera is idle, but there is a roughly 3° C step between these periods. This bimodal behavior will be the subject of further development, although the current performance would be perfectly acceptable using a small correction for the temperature-dependent gain.

Figure 13. CCD (top) and REB (bottom) temperature vs. time over a 16 day period of Camera operation in November 2023, for one CCD and REB per Science Raft.

4.5 CCD & Focal Plane Effects

During the course of the electro-optical testing we have also continually optimized the CCD and Focal Plane performance, as described in a companion proceeding in a parallel conference.[13] In addition we have observed a range of CCD features and have characterized these further both to understand the Camera operation but also to guide us in the development of correction algorithms in the Rubin Data Management ISR. Recent publications describe detailed results on tree rings and other pixel size effects[14] and the so-called brighter-fatter effect that broadens the PSF as the flux increases from electrostatic repulsion.[15]

To illustrate the range of observations made with Camera test data we show a gallery of addition Focal Plane and CCD effects in Figure 14. The effects include: a small level of persistence in the e2v CCD-250 CCDs following an image with saturated pixels, temporal variations in the bias as seen in a plot of the projected bias level in the serial direction, correlated read noise, and evidence for small temporal variations of throughput due to turbulence of air inside the Camera body.[16] In addition a detailed study of cross talk and nonlinearity in the observed cross talk will be published soon.[17]

5. CONCLUSIONS

Verification testing of the LSST Camera at SLAC was completed in March 2024 and the Camera was shipped to the Rubin Observatory on Cerro Pachon in May 2024. The Camera will be commissioned in the dome facility clean room to reestablish nominal operating conditions, verify a few remaining requirements pertaining to the Guider and DAQ operation and target several remaining Focal Plane optimization targets. In the fourth quarter of 2024 the Camera is schedule to be installed on the Simonyi Survey Telescope with on-sky commissioning to follow. The 10-year LSST is scheduled to begin in the middle of calendar 2025.

ACKNOWLEDGMENTS

This material is based upon work supported in part by the National Science Foundation through Cooperative Agreement 1258333 managed by the Association of Universities for Research in Astronomy (AURA), and the Department of Energy under Contract No. DE-AC02-76SF00515 with the SLAC National Accelerator Laboratory. Additional Rubin funding comes from private donations, grants to universities, and in-kind support from LSSTC Institutional Members.

REFERENCES

[1] Ivezić, Ž., Kahn, S. M., Tyson, J. A., and others for the LSST Collaboration, "LSST: from Science Drivers to Reference Design and Anticipated Data Products," *ArXiv e-prints* , arXiv:0805.2366 (May 2018).

[2] Ivezic, Z. and the LSST Science Collaboration, "Science Requirements Document, LPM-17." https://docushare.lsstcorp.org/docushare/dsweb/Get/LPM-17 (2018). (Accessed: 17 June 2024).

[3] Roodman, A., Bogart, J. R., Bond, T., Borgland, A. W., Chiang, J., Digel, S. W., Dubois, R., Focke, W. B., Glanzman, T., Gilmore, K., Hascall, D., Hascall, P., Herrmann, S., Johnson, A. S., Kelly, H. M., Lange, T., Lopez, M., Marshall, S., Neal, H., Newbry, S., Nordby, M., Rasmussen, A., Reil, K., Rosenberg, E., Russo, S., Saxton, O., Snyder, A., Tether, S., Turri, M., Utsumi, Y., O'Connor, P., Nomerotski, A., Rumore, M., Haupt, J., Takacs, P., Barrau, A., Combet, C., Dargaud, G., Eraud, L., Marton, M., Migliore, M., Perbet, E., Ricol, J. S., Vescovi, C., Doherty, P., Baumann, B., Winters, S., Wolfe, J., Antilogus, P., and Juramy, C., "Integration and verification testing of the LSST camera," in [*Modeling, Systems Engineering, and Project Management for Astronomy VIII*], Angeli, G. Z. and Dierickx, P., eds., *Society of Photo-Optical Instrumentation Engineers (SPIE) Conference Series* **10705**, 107050D (July 2018).

[4] Bond, T., Roodman, A., Reil, K., Lange, T., Nordby, M., Newbry, S., Lopez, M., Bowdish, B., Lee, V., Hascall, D., Munoz, J., Marshall, S., Rasmussen, A., Digel, S., Utsumi, Y., and Snyder, A., "LSST camera - integration and test subsystem: planning and status," in [*Modeling, Systems Engineering, and Project Management for Astronomy VIII*], Angeli, G. Z. and Dierickx, P., eds., *Society of Photo-Optical Instrumentation Engineers (SPIE) Conference Series* **10705**, 107050E (July 2018).

[5] Lange, T. t., "Building the LSST camera," Proc. SPIE **13096**, in press (2024).

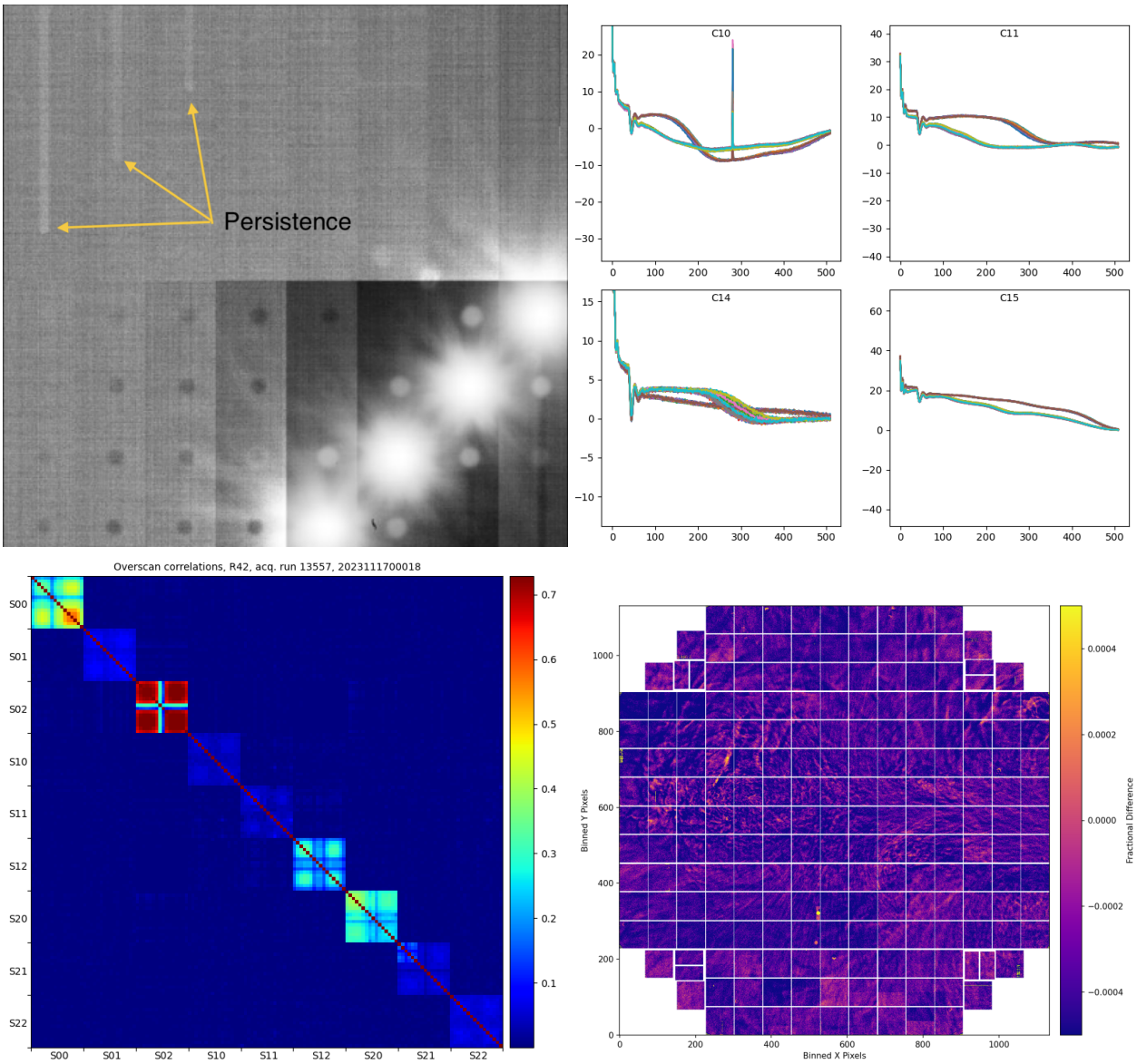

Figure 14. A gallery of Focal Plane effects from the LSST Camera testing program. Persistence in e2v CCDs, as seen in remnants from the previous image (top left). Serial profile of bias images showing a multiple families of bias levels (top right). Correlations in overscan values between amplifier channels of a representative Science Raft (bottom left). Turbulence patterns seen comparing the flux in a single short flat image with the average of many flat images (bottom right).

[6] Lopez, M., Marshall, S., Bond, T., Haupt, J., Johnson, T., Neal, H., O'Connor, P., Rasmussen, A., Roodman, A., Takacs, P., and Utsumi, Y., "Acceptance testing for LSST camera raft tower modules," in [*Ground-based and Airborne Instrumentation for Astronomy VII*], Evans, C. J., Simard, L., and Takami, H., eds., *Society of Photo-Optical Instrumentation Engineers (SPIE) Conference Series* **10702**, 107022C (July 2018).

[7] Kotov, I. V., Haupt, J., O'Connor, P., Smith, T., Takacs, P., Neal, H., and Chiang, J., "Characterization and acceptance testing of fully depleted thick CCDs for the large synoptic survey telescope," in [*High Energy, Optical, and Infrared Detectors for Astronomy VII*], Proc. SPIE **9915**, 99150V (July 2016).

[8] O'Connor, P., Antilogus, P., Doherty, P., Haupt, J., Herrmann, S., Huffer, M., Juramy-Giles, C., Kuczewski, J., Russo, S., Stubbs, C., and Van Berg, R., "Integrated system tests of the LSST raft tower modules," in

[*High Energy, Optical, and Infrared Detectors for Astronomy VII*], Proc. SPIE **9915**, 99150X (July 2016).

[9] Rasmussen, A., "Focal plane figure - knowledge and control for rubin observatory's lsst camera." Image Sensors for Precision Astronomy, Poster Session https://indico.slac.stanford.edu/event/8442/contributions/8615/ (2024). (Accessed: 17 June 2024).

[10] Antilogus, P., Aubourg, É., Boucaud, A., Breugnon, P., Coridian, J., Croizet, H., Daubard, G., Gallo, F., Juramy, C., Karst, P., Kusulja, M., Labat, D., Lagorio, E., Laporte, D., Marini, A., Verdier, P., Vezzu, F., Virieux, F., and Weicherding, T., "Design, assembly and validation of the Filter Exchange System of LSSTCam," in [*Ground-based and Airborne Telescopes IX*], Marshall, H. K., Spyromilio, J., and Usuda, T., eds., *Society of Photo-Optical Instrumentation Engineers (SPIE) Conference Series* **12182**, 121823A (Aug. 2022).

[11] Snyder, A., Barrau, A., Bradshaw, A., Bowdish, B., Chiang, J., Combet, C., Digel, S., Dubois, R., Eraud, L., Juramy, C., Lage, C., Lange, T., Migliore, M., Nomerotski, A., O'Connor, P., Park, H. Y., Rasmussen, A., Reil, K., Roodman, A., Shestakov, A., Utsumi, Y., and Wood, D., "Laboratory measurements of instrumental signatures of the LSST camera focal plane," in [*X-Ray, Optical, and Infrared Detectors for Astronomy IX*], Holland, A. D. and Beletic, J., eds., *Society of Photo-Optical Instrumentation Engineers (SPIE) Conference Series* **11454**, 1145439 (Dec. 2020).

[12] Astier, P., Antilogus, P., Juramy, C., Le Breton, R., Le Guillou, L., and Sepulveda, E., "The shape of the photon transfer curve of CCD sensors," A&A **629**, A36 (Sept. 2019).

[13] Utsumi, Y. t., "LSST Camera Focal Plane Optimization," Proc. SPIE **13103**, in press (2024).

[14] Esteves, J. H., Utsumi, Y., Snyder, A., Schutt, T., Broughton, A., Trbalic, B., Mau, S., Rasmussen, A., Plazas Malagón, A. A., Bradshaw, A., Marshall, S., Digel, S., Chiang, J., Rykoff, E., Waters, C., Soares-Santos, M., and Roodman, A., "Photometry, Centroid and Point-spread Function Measurements in the LSST Camera Focal Plane Using Artificial Stars," PASP **135**, 115003 (Nov. 2023).

[15] Broughton, A., Utsumi, Y., Plazas Malagón, A. A., Waters, C., Lage, C., Snyder, A., Rasmussen, A., Marshall, S., Chiang, J., Murgia, S., and Roodman, A., "Mitigation of the Brighter-fatter Effect in the LSST Camera," PASP **136**, 045003 (Apr. 2024).

[16] Banovetz, J., "*Weather* in lsst camera: Characterizing turbulence as seen in flat illuminated images." Image Sensors for Precision Astronomy, Poster Session https://indico.slac.stanford.edu/event/8442/contributions/8587/ (2024). (Accessed: 17 June 2024).

[17] Liang, S., "Measuring the delayed crosstalk." Image Sensors for Precision Astronomy, Poster Session https://indico.slac.stanford.edu/event/8442/contributions/8929/ (2024). (Accessed: 17 June 2024).